J Mater Sci (2022) 57:19946–19956

Energy materials

Polyoxometalate embedded in metal–organic framework surface building strong polysulfides barrier for high-performance Li–S batteries

Wenjie Li[1], Xiujing Luan[1], Xiaoxue Zhu[1], Jian Sun[2], and Linlin Fan[3,*]

[1] Shandong Baichuan Intelligent Technology Co., Ltd., Jinan 250022, China
[2] Shandong Lubi Building Materials Co., Ltd., Jinan 250022, China
[3] Collaborative Innovation Center of Metal Nanoclusters & Photo/Electro-Catalysis and Sensing, School of Materials Science and Engineering, University of Jinan, Jinan 250022, China

Received: 31 May 2022
Accepted: 25 October 2022
Published online: 2 November 2022

ABSTRACT

The elaborate design of functional separators is considered as an effective and economical approach to accelerate the conversion of sulfur species and inhibit shuttling effect of soluble lithium polysulfides (LiPSs). This work chooses ZIF-67 and $H_5PW_{10}V_2O_{40}{\cdot}30H_2O$ ($PW_{10}V_2$) as the precursors to construct MOF/POM composite by electrostatic interaction as the modified material of separator in lithium–sulfur (Li–S) batteries. ZIF-67 with suitable size window of micropores functions as a physical barrier to hinder polysulfides shuttling, while lithium ions can flow freely across the modified separator. Furthermore, $PW_{10}V_2$ presents firm chemical anchoring for LiPSs and displays excellent catalytic activity for polysulfides, which is conducive to preventing the soluble polysulfides from reaching lithium anode and kinetically facilitating sulfur redox reaction kinetics. Consequently, Li–S cells with ZIF-67/$PW_{10}V_2$-modified functional separators display an initial discharge capacity of 1637.6 mAh g^{-1} under 0.2 C. After 120 cycles, superior reversible capacities of 1054.6 mAh g^{-1} under 0.5 C and 802.7 mAh g^{-1} under 2 C can still be maintained.

Handling Editor: Mark Bissett.

Address correspondence to E-mail: mse_fanll@ujn.edu.cn

https://doi.org/10.1007/s10853-022-07881-7

GRAPHICAL ABSTRACT

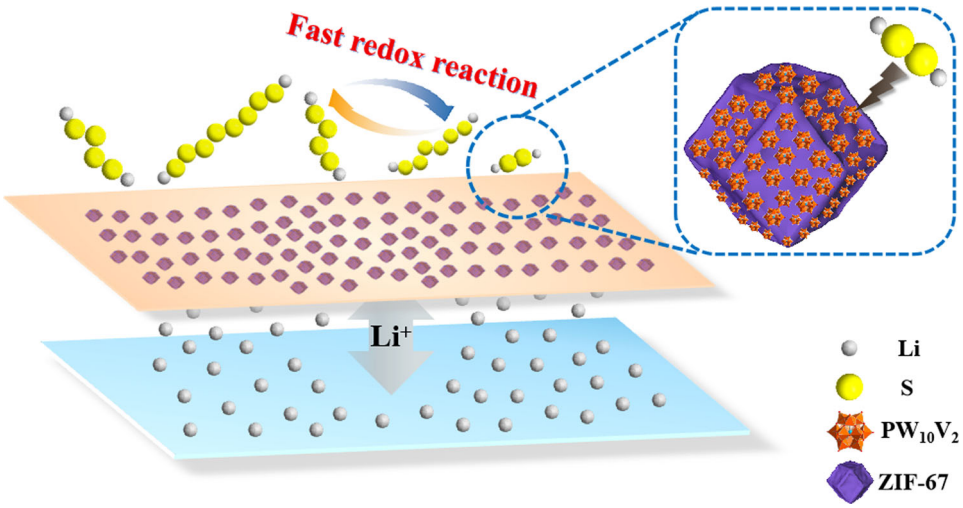

Introduction

Lithium–sulfur (Li–S) batteries with superior theoretical specific capacity, environmental-friendliness and low cost are the hopeful next-generation energy storage systems [1–3]. However, the practical application of Li–S batteries is plagued by many technical bottlenecks; especially, the shuttle effect induced by dissolution of the lithium polysulfides (LiPSs) leads to sluggish redox kinetics and worse sulfur utilization [4–6]. Actually, the generated polysulfides can spread from cathode to anode, and polysulfides are reduced to insoluble Li_2S [7]. Therefore, utilizing a functional interlayer between separator and sulfur cathode to hinder shuttling is a feasible strategy [8–10].

The metal–organic frameworks (MOFs) are composed of metal ions and organic ligands [11–13], which are a kind of porous materials developed recently and have been employed as host matrixes for sulfur cathode (such as MIL-101, ZIF-8 and MOF-525) [14–16]. However, the skeleton gradually degrades during long time cycling and is unable to restrain soluble polysulfides. Besides, insulating nature of MOFs and sulfur also hampers their success. Notably, the use of MOFs with highly ordered pores and large surface area in Li–S cells as modified materials of separator may be a suitable choice [17–19]. The size window of micropores in MOFs can be regulated to ensure the free migration of lithium ions, but prevent the transfer of polysulfides. Therefore, MOFs-modified separator is expected to establish a reliable physical barrier to mitigate severe shuttle effect of polysulfides [20]. Note that although MOFs with suitable pore size have the blocking effect on polysulfides, the slow redox kinetics of sulfur species during cycling cannot be conquered, which has certain limitations to meet the practical requirement [21, 22].

Polyoxometalates (POMs) are a type of anionic clusters connected by shared oxygen atoms to form well-defined cluster frameworks, which display the feasibility of efficient catalysts in biomass oxidation and photocatalysis [23, 24]. Moreover, because POMs have the ability of rapid redox reaction and transferring multiple electrons on per molecule, they have become the potential electrode materials for green energy devices [25, 26]. Interestingly, POMs have been found that they can immobilize polysulfides and accelerate transfer of soluble high-order Li_2S_x ($4 \leq x \leq 8$) to Li_2S_2/Li_2S, thus the reaction kinetics of polysulfides is extremely enhanced [27]. According to previous reports [28, 29], it can be concluded that W-containing POMs present appropriate redox potentials, which cover the range of equilibrium

potentials of sulfur redox reactions, and thus is more conducive to enhancing the electrochemical property of Li–S batteries [30].

Given these observations, this work chooses $H_3[PW_{12}O_{40}]xH_2O$ (PW_{12}), $H_4PW_{11}VO_{40}{\cdot}8H_2O$ ($PW_{11}V$), and $H_5PW_{10}V_2O_{40}{\cdot}30H_2O$ ($PW_{10}V_2$) as POMs as well as ZIF-67 as MOF precursor to construct the MOF/POM composites used as modified materials of separator, in which POMs are tightly and uniformly attached to the surface of ZIF-67 by electrostatic attraction. ZIF-67 exhibits highly ordered micropores with a size window of 0.34 nm, which is remarkably smaller than molecular size of LiPSs, so it is ideal to obstruct polysulfides as a physical barrier. Moreover, $PW_{10}V_2$ with strong chemisorption ability and catalytic activity can further inhibit shuttle effect as well as enhance the redox kinetics of LiPSs. Li–S cells with ZIF-67/$PW_{10}V_2$-modified separators obtain a superior initial discharge specific capacity of 1637.6 mAh g^{-1} under 0.2 C. Meanwhile, it can reach up to 1054.6 mAh g^{-1} under 0.5 C and still retain 802.7 mAh g^{-1} under 2 C upon 120 cycles.

Experimental section

Preparation of ZIF-67

2.5 mmol $Co(NO_3)_2{\cdot}6H_2O$ and 19.8 mmol 2-methylimidazole were added into 120 mL methanol under magnetic stirring, respectively. Afterward, mixing the above solutions quickly and stirring for another 24 h. The as-synthesized product was washed several times with distilled water and methanol by centrifugation. Finally, the resulting products were dried at 80 °C.

Synthesis of MOF/POM composites

One hundred milligrams of pre-prepared ZIF-67 was added into 40 mL methanol under magnetic stirring at 40 °C for 12 h, denoted as solution A. Sixty milligrams of PW_{12}, $PW_{11}V$ and $PW_{10}V_2$ was added in 40 mL methanol solution, respectively, denoted as solution B. Subsequently, the mixed solution (including A and B) was transferred to Teflon-lined stainless steel autoclave and heated under 100 °C for 6 h. Finally, the obtained products were washed several times with distilled water and methanol by centrifuge separation and dried under 70 °C. Three final products were marked as ZIF-67/PW_{12}, ZIF-67/$PW_{11}V$ and ZIF-67/$PW_{10}V_2$, respectively.

Synthesis of MOF/POM-modified separator

MOF/POM composites, Super P and polyvinylidene fluoride (PVDF) were added in N-methyl-2-pyrrolidinone (NMP) at a mass ratio of 7:2:1 under vigorous stirring to generate a uniform slurry, which was then coated on pristine Celgard 2500 (PP) separator. The obtained functionalized separator was dried under 50 °C. Finally, modified functional separators were cut into discs with a diameter of 16 mm. The mass loading of modified material in separator was 0.43 mg cm^{-2}.

Results and discussion

Figure S1 shows that ZIF-67 with the diameter size of 400 nm presents the regular dodecahedron structure. Afterward, PW_{12}, $PW_{11}V$ and $PW_{10}V_2$ are evenly distributed on the surface of ZIF-67 via electrostatic attraction by one-step hydrothermal treatment, and the resulting composites are marked as ZIF-67/PW_{12}, ZIF-67/$PW_{11}V$ and ZIF-67/$PW_{10}V_2$, respectively. Morphology and structure of three MOF/POM composites are presented via SEM and TEM (Fig. 1a–c). One can see that the skeleton of ZIF-67 is etched to a certain extent during hydrothermal treatment due to the strong acidity of POMs, while three MOF/POM composites still maintain a relatively complete skeleton structure. In Fig. 1d–f, one can see from FTIR that the main peak positions of POMs and ZIF-67 do not change significantly after hydrothermal treatment. The characteristic peaks at 1579, 1430, 1139, 993 and 424 cm^{-1} correspond with C = N, –CH_3, C–N, N–H and Co–N groups of ZIF-67; meanwhile, peaks at 1078, 956, 890 and 827 cm^{-1} are in accord with P–O_a, W = O_d, W–O_b–W and W–O_c–W groups of POMs [15, 16, 31]. These results confirm the successful combination of POMs and ZIF-67, which is in correspondence with XRD patterns (Fig. S2). To visually explore trapping effect of three MOF/POM composites toward polysulfides, adsorption experiments of Li_2S_6 solutions is carried out in parallel (Fig. 1g). After being adsorbed by the ZIF-67/$PW_{10}V_2$, the solution changes from a dark brown to almost colorless, and the adsorption capacity of MOF/POM composites is in the following order: ZIF-

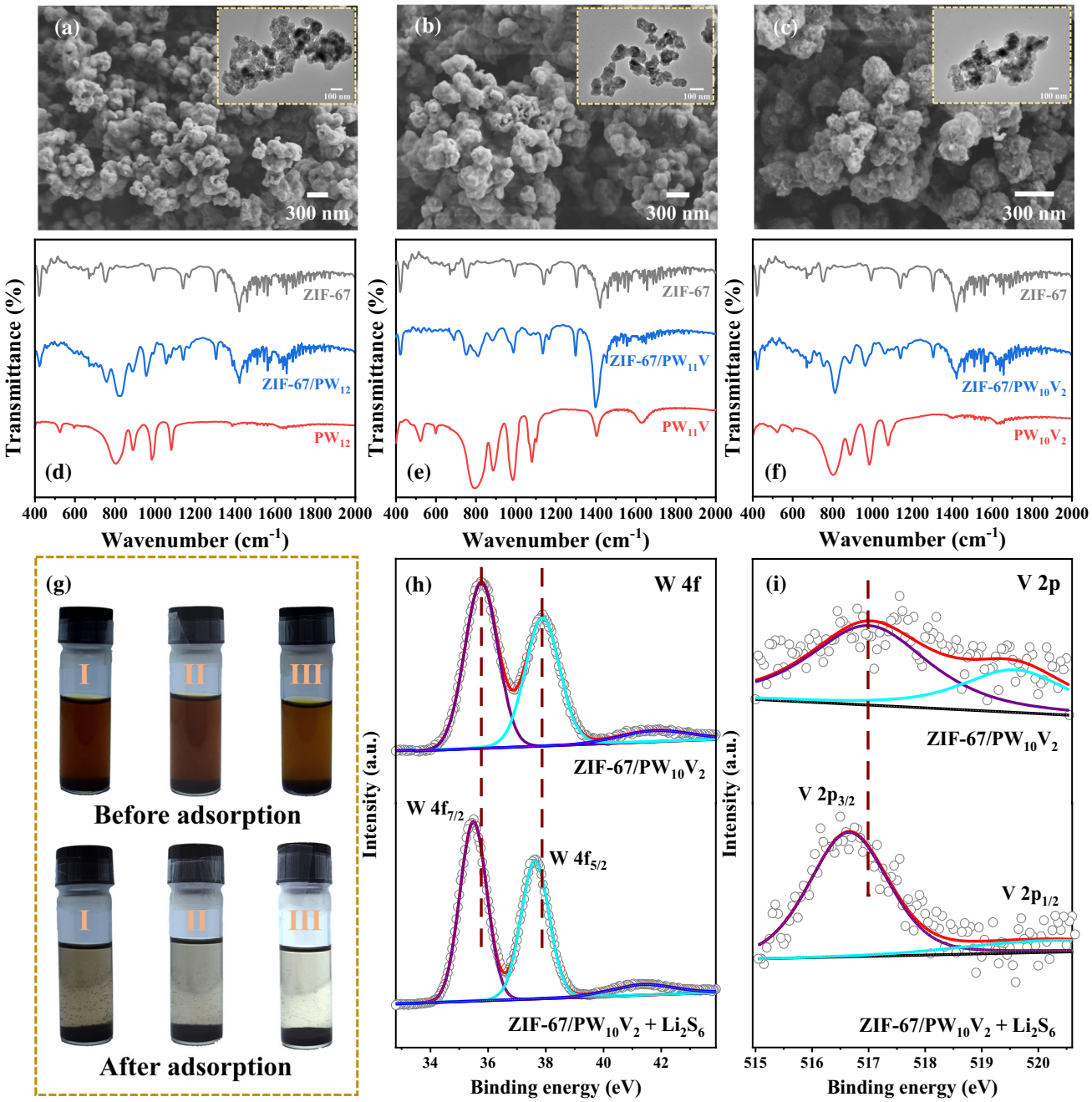

Figure 1 SEM images of **a** ZIF-67/PW_{12}, **b** ZIF-67/$PW_{11}V$ and **c** ZIF-67/$PW_{10}V_2$ (the inserts are TEM images); FTIR spectra of **d** ZIF-67/PW_{12}, **e** ZIF-67/$PW_{11}V$ and **f** ZIF-67/$PW_{10}V_2$; **g** Optical observation of Li_2S_6 solution adsorbed by ZIF-67/PW_{12} (I), ZIF-67/$PW_{11}V$ (II) and ZIF-67/$PW_{10}V_2$ (III); XPS analysis of ZIF-67/$PW_{10}V_2$ and ZIF-67/$PW_{10}V_2$ + Li_2S_6: **h** W 4f spectra and **i** V 2p spectra.

67/$PW_{10}V_2$ > ZIF-67/$PW_{11}V$ > ZIF-67/PW_{12}, demonstrating more firm anchoring of $PW_{10}V_2$ toward polysulfides. Based on the analysis of the supernatant, an obvious peak at approximately 280 nm appears in the UV–Vis spectra before adsorption (Fig. S3). The peak intensity significantly weakens when Li_2S_6 solution is adsorbed by MOF/POM. Particularly, ZIF-67/$PW_{10}V_2$ presents the weakest absorption peaks, which further indicates the strong adsorption capacity of $PW_{10}V_2$.

Moreover, XPS tests are utilized to investigate the chemical interactions between LiPSs and ZIF-67/

$PW_{10}V_2$ adsorbent [25]. For pristine ZIF-67/$PW_{10}V_2$, two fitted peaks at 35.8 eV and 37.6 eV are in accord with W $4f_{7/2}$ and W $4f_{5/2}$ of W (VI) (Fig. 1h), and the fitted peaks at 516.9 eV and 519.6 eV agree well with V $2p_{3/2}$ and V $2p_{1/2}$ of V (VI) (Fig. 1i). Note that the spectra peaks of W 4f and V 2p shift to the lower binding energies after interacting with Li_2S_6 [12], while no significant change is found for Co 2p and P 2p spectra (Fig. S4), confirming that the adsorption behavior of LiPSs is mainly caused by $PW_{10}V_2$ [7, 15, 22, 32]. For S 2p spectra of ZIF-67/$PW_{10}V_2$- + Li_2S_6 (Fig. S5), the double peaks at 161.7 eV and 162.0 eV correspond with the terminal sulfur (S_T) of Li_2S_6, the double peaks at 163.0 eV and 163.9 eV are related to the bridging sulfur (S_B) of Li_2S_6, and other two double peaks at high binding energies are in accord with thiosulfate and polythionate, respectively. Note that the spectra peaks positively shift by 0.13 eV for S_B and 0.43 eV for S_T compared to the bare Li_2S_6, confirming the strong chemical capture of ZIF-67/$PW_{10}V_2$ toward LiPSs [22, 33]. Nitrogen adsorption/desorption tests are performed to further confirm the texture properties of ZIF-67/$PW_{10}V_2$, as shown in Fig. S6. The BET surface area is estimated to be 1171 $m^2\ g^{-1}$. Additionally, the pore size of approximately 1.1 nm is determined, featuring a superior micropore property.

Subsequently, the designed MOF/POM composites as modification layers are scraped onto surface of separators. Taking ZIF-67/$PW_{10}V_2$ as an example, ZIF-67/$PW_{10}V_2$ coating thickness is approximately 5.4 μm (Fig. 2a). No visible crack can be found on the surface of separator in the folding process, suggesting the excellent structural flexibility and ruggedness (Fig. 2b). The element mappings prove that C, Co, N, P, W, V and O elements are uniformly dispersed on separator (Fig. S7), which is in accord with the dark-field STEM image and EDX mapping (Fig. S8). Meanwhile, the XRD result of ZIF-67/$PW_{10}V_2$-modified separator agrees well with the XRD pattern of ZIF-67/$PW_{10}V_2$ (Fig. S9), suggesting the stable existence of ZIF-67 and $PW_{10}V_2$ after coating process. The contact angle tests are carried out by dripping electrolyte on the pristine PP separator and ZIF-67/$PW_{10}V_2$-modified separator (Fig. S10). Obviously, the contact angle of ZIF-67/$PW_{10}V_2$-modified separator is smaller than that of PP separator, illustrating the ZIF-67/$PW_{10}V_2$-modified separator with rich voids greatly increases the wettability of electrolyte, which is beneficial to reduce the interface concentration

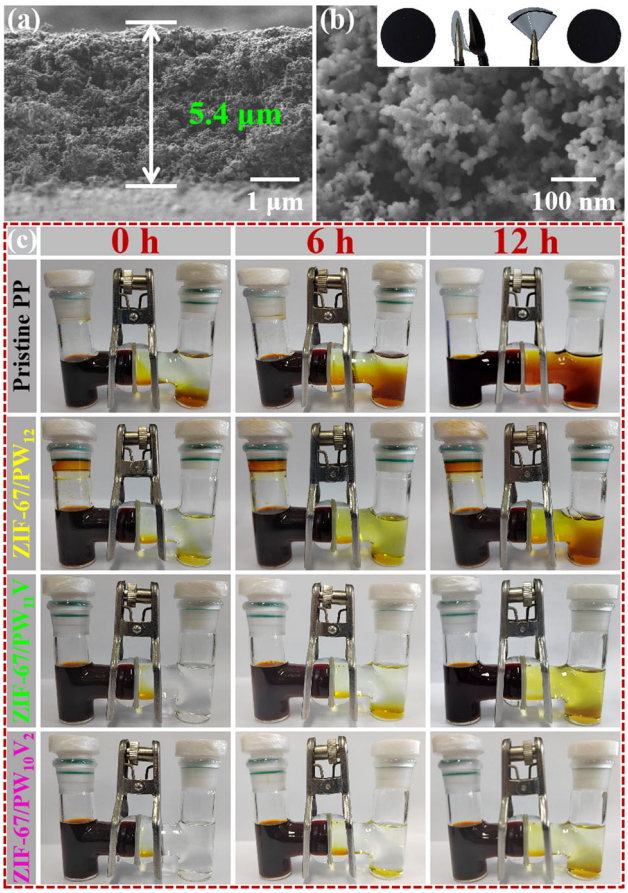

Figure 2 **a** The cross section and **b** the top surface SEM images of ZIF-67/$PW_{10}V_2$-modified separator (the insert shows the folding process of ZIF-67/$PW_{10}V_2$-modified separator); **c** The penetration test with the pristine PP separator, ZIF-67/PW_{12}, ZIF-67/$PW_{11}V$ and ZIF-67/$PW_{10}V_2$-modified separators at different time.

gradient during lithium ions transmission. Li_2S_6 solution penetration test is performed by a H-type cell configuration. One can see from Fig. 2c that 0.1 M Li_2S_6 solution (left) and bare DME/DOL (1:1 in volume) solvent (right) are separated by different separators. The pristine PP separator undergoes severe Li_2S_6 penetration, and the DME/DOL solvent renders a yellow–brown color after 12 h. As expected, Li_2S_6 penetration is effectively suppressed by MOF/POM-modified separators; especially, only a slight color change is observed for the DME/DOL electrolyte in the right chamber using ZIF-67/$PW_{10}V_2$-modified separator after 12 h.

Li–S batteries with MOF/POM-modified separator and S/KB cathode are assembled to test electrochemical property. Morphological feature of S/KB is measured by SEM (Fig. S11), and sulfur loading in

cathode material is 68.6 wt% (Fig. S12). Figure S13 shows CV curves of cells with ZIF-67/PW_{12}-, ZIF-67/$PW_{11}V$- and ZIF-67/$PW_{10}V_2$- modified separators ranging from 1.7 V to 2.8 V at a scan rate of 0.1 mV s^{-1}. Two obvious discharge platforms at 2.23 V and 2.01 V correspond with reduction of sulfur to long-chain LiPSs and further reduction to solid Li_2S_2/Li_2S. Charge plateau at 2.43 V is consistent with the oxidation of Li_2S_2/Li_2S to long-chain polysulfides as well as final formation of sulfur [34]. The initial charge/discharge voltage curves of ZIF-67/PW_{12}-, ZIF-67/$PW_{11}V$- and ZIF-67/$PW_{10}V_2$-modified separators under 0.2 C are presented in Fig. 3a. Clearly, compared with ZIF-67/PW_{12} (1509.6 mAh g^{-1}) and ZIF-67/$PW_{11}V$ (1550.8 mAh g^{-1}), the ZIF-67/$PW_{10}V_2$-modified separator possesses the superior discharge capacity of 1637.6 mAh g^{-1} (this value is close to theoretical specific capacity of the sulfur cathode). In addition, ZIF-67/$PW_{10}V_2$-modified separator displays a lower polarization value of 116 mV than that of ZIF-67/$PW_{11}V$ (161 mV) and ZIF-67/PW_{12} (208 mV), suggesting decreased voltage hysteresis and fast redox reaction kinetics of cells based on ZIF-67/$PW_{10}V_2$. Figure 3b exhibits galvanostatic discharge/charge experiments of ZIF-67/$PW_{10}V_2$-based cells at current densities of 0.2–2 C. It delivers reversible capacities of 1637.6, 1502.6, 1290.5 and 1071.5 mAh g^{-1} under 0.2 C, 0.5 C, 1 C and 2 C, respectively, showing outstanding electrochemical performance. Furthermore, cycling performance of Li–S cells with MOF/POM-modified separators is performed at current densities of 0.2 C (Fig. 3c). ZIF-67/$PW_{10}V_2$-modified separator delivers an excellent reversible capacity of 1149.7 mAh g^{-1} after 120 cycles. However, the reversible capacities of ZIF-67/$PW_{11}V$- and ZIF-67/PW_{12}-modified separators drastically decline to 979.6 mAh g^{-1} and 946.3 mAh g^{-1} in the 120th cycle. As current density raises to 0.5 C (Fig. 3d), initial discharge capacity of 1502.6 mAh g^{-1} is obtained for ZIF-67/$PW_{10}V_2$-modified separator and is still remained at 1054.6 mAh g^{-1} upon 120 cycles. In contrast, ZIF-67/$PW_{11}V$- and ZIF-67/PW_{12}-modified separators display poor performances with reversible capacities of 962.8 mAh g^{-1} and 910.3 mAh g^{-1} in the 120th cycle. To testify cycling stability at higher discharge rates [35], we cycle cells with ZIF-67/$PW_{10}V_2$-modified separator at 1 C and 2 C (Fig. 3e, f). As expected, it can reach up to 876.5 mAh g^{-1} at 1 C and still maintain 802.7 mAh g^{-1} under 2 C after 120 cycles. Figure S14 shows the comparison of rate capability of cells with three MOF/POM-modified separators. Clearly, ZIF-67/$PW_{10}V_2$-modified separator delivers the superior discharge capacities of 1636.5, 1262.2, 1081.8, 956.8 and 785.2 mAh g^{-1} at different current densities of 0.2 C, 0.5 C, 1.0 C, 2.0 C and 3.0 C, respectively. When the current density decreases back to 0.2 C, the discharge capacity can recover to 1254.6 mAh g^{-1}. Furthermore, the comparison of electrochemical performance of cell with ZIF-67/$PW_{10}V_2$-modified separator and other modified materials reported in the previous literatures is listed in Table S1. Outstanding electrochemical property demonstrates high sulfur utilization by the ZIF-67/$PW_{10}V_2$ as a physical barrier, and $PW_{10}V_2$ with effective catalytic activity and strong capture ability for LiPSs is more beneficial to accelerate redox kinetics of sulfur species during discharge/charge process [36].

Moreover, the morphology characterization of lithium anode after 50 cycles at 1 C is recorded (Fig. S15). The surface of lithium anode presents the obvious sulfur species for the cell with bare PP separator. Fortunately, there is no obvious sulfur species when the separators are modified by three MOF/POM composites, confirming that MOF/POM materials can prevent polysulfides from reaching the lithium anode, especially ZIF-67/$PW_{10}V_2$. To further illustrate the structure and component of ZIF-67/$PW_{10}V_2$ composites upon cycling, the electrochemical cell with ZIF-67/$PW_{10}V_2$-modified separator is disassembled in the argon-filled glovebox. It can be seen from Fig. S16 that the morphology and structure of ZIF-67/$PW_{10}V_2$ are almost maintained. FTIR, XRD and XPS results show the stable existence of ZIF-67 and $PW_{10}V_2$ during the repeated charging and discharging (Fig. S17 ~ S19).

To further explore diffusion behavior of lithium ion in the electrode materials, CV measurements with different scan speeds are recorded (Fig. 4a-c). Lithium ion diffusion coefficient is calculated via Randles–Sevcik equation [20]:

$$I_p = 2.69 \times 10^5 n^{3/2} A D^{1/2} C v^{1/2}$$

A is geometric area of cathode, D represents lithium ion diffusion coefficient, I_p represents peak current, n refers to electron number, C represents lithium ion concentration, and v refers to scan rate. There is a linear relationship for I_p and $v^{1/2}$, and resulting slope is related to lithium ion diffusion

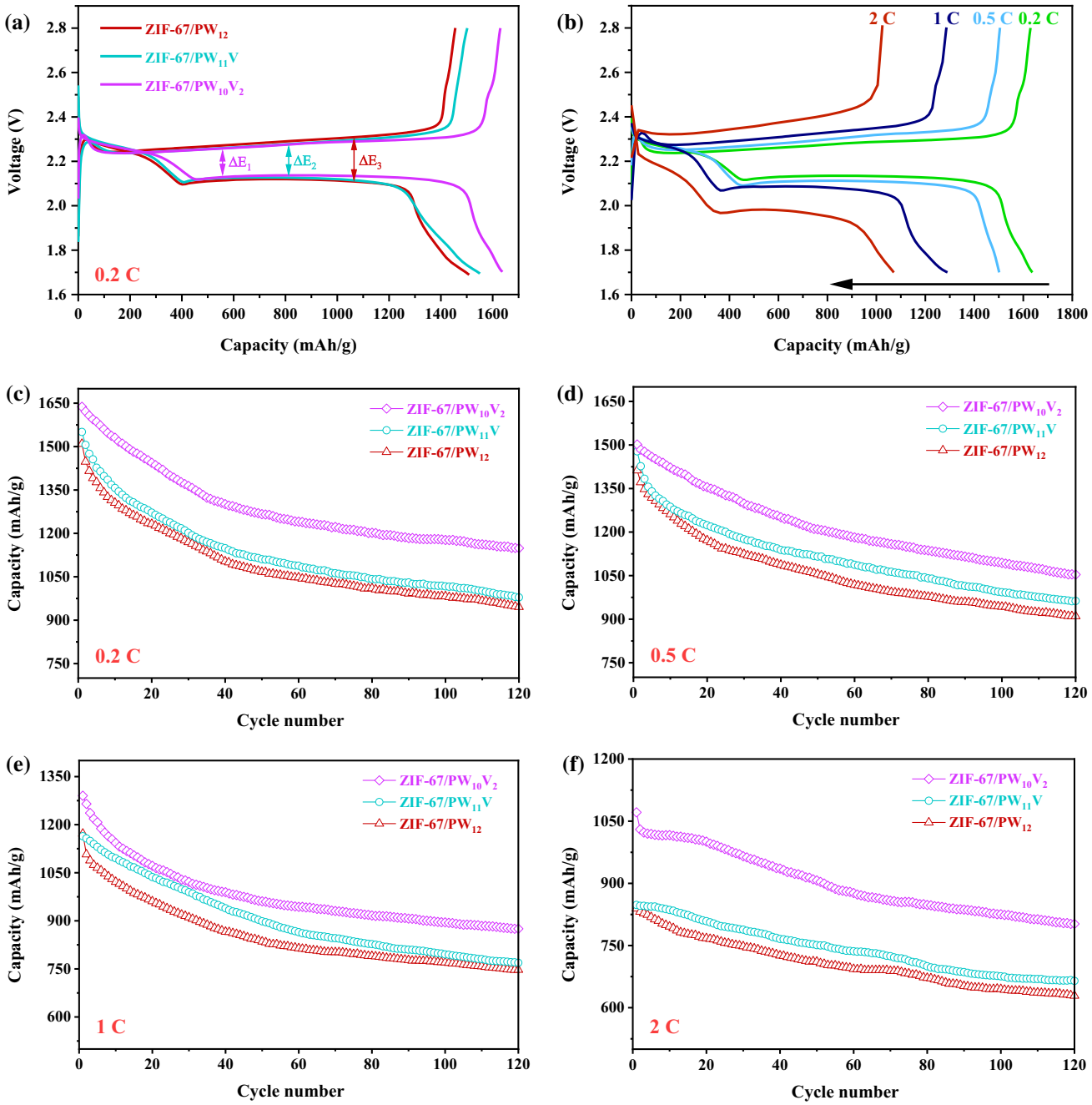

Figure 3 **a** Initial galvanostatic charge/discharge profiles of ZIF-67/PW_{12}-, ZIF-67/$PW_{11}V$- and ZIF-67/$PW_{10}V_2$-modified separators at 0.2 C; **b** initial galvanostatic charge/discharge profiles of ZIF-67/$PW_{10}V_2$-modified separator at current densities from 0.2 C to 2 C; cycling performance of ZIF-67/PW_{12}-, ZIF-67/$PW_{11}V$- and ZIF-67/$PW_{10}V_2$-modified separators at **c** 0.2 C, **d** 0.5 C, **e** 1 C and **f** 2 C.

ability. As displayed in Fig. 4d, one can see that the cell with ZIF-67/$PW_{10}V_2$-modified separator exhibits the highest slopes among the three samples, suggesting that $PW_{10}V_2$ can facilitate catalytic effect for polysulfides conversion and decrease lithium ion transfer barrier. EIS is performed to obtain a more thorough insight into electrochemical behaviors of cells with MOF/POM-modified separators (Fig. 5a), and the corresponding equivalent circuit diagram is illustrated in Fig. S20. Obviously, ZIF-67/$PW_{10}V_2$-modified separator presents a lower charge transfer resistance (38 Ω) compared with ZIF-67/$PW_{11}V$ (59 Ω) and ZIF-67/PW_{12} (67 Ω), suggesting the enhanced electrochemical kinetics. Warburg coefficient, which

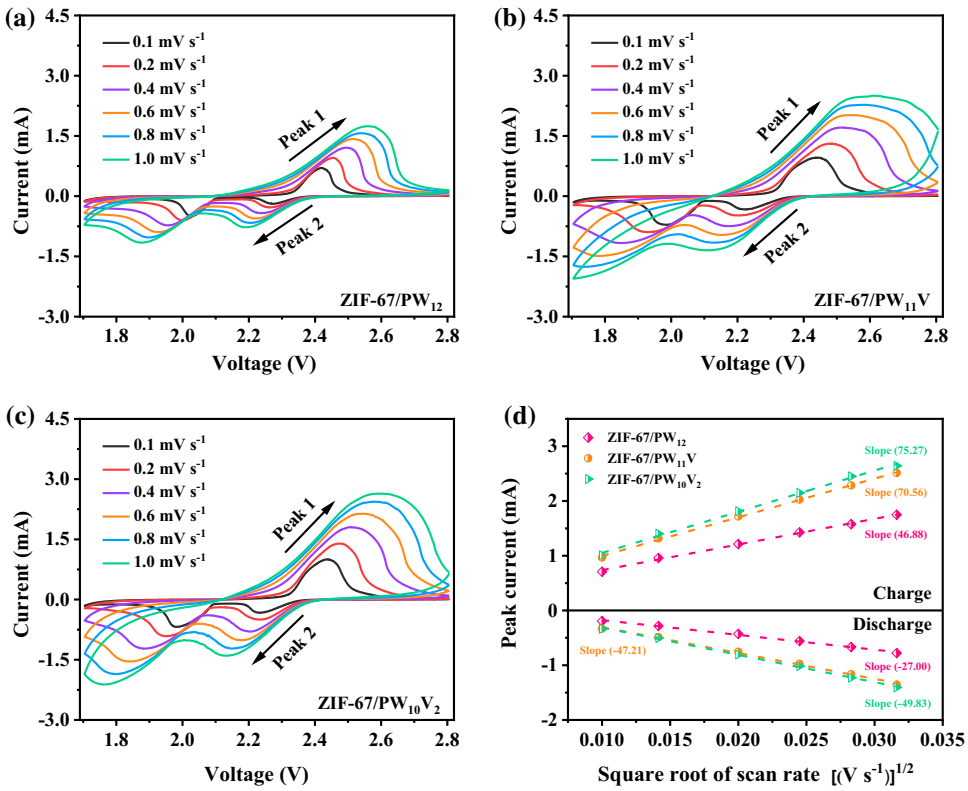

Figure 4 CV curves of **a** ZIF-67/PW_{12}-, **b** ZIF-67/$PW_{11}V$- and **c** ZIF-67/$PW_{10}V_2$-modified separators at different scan rates (the coin cell is assembled with as-prepared sample as working electrode, metallic lithium foil as the counter and reference electrodes, and 1 M LiTFSI in DOL/DME (1:1 by volume) with 1 wt% $LiNO_3$ as electrolyte); **d** plots of the peak current versus the square root of scan rate for ZIF-67/PW_{12}-, ZIF-67/$PW_{11}V$- and ZIF-67/$PW_{10}V_2$-modified separators.

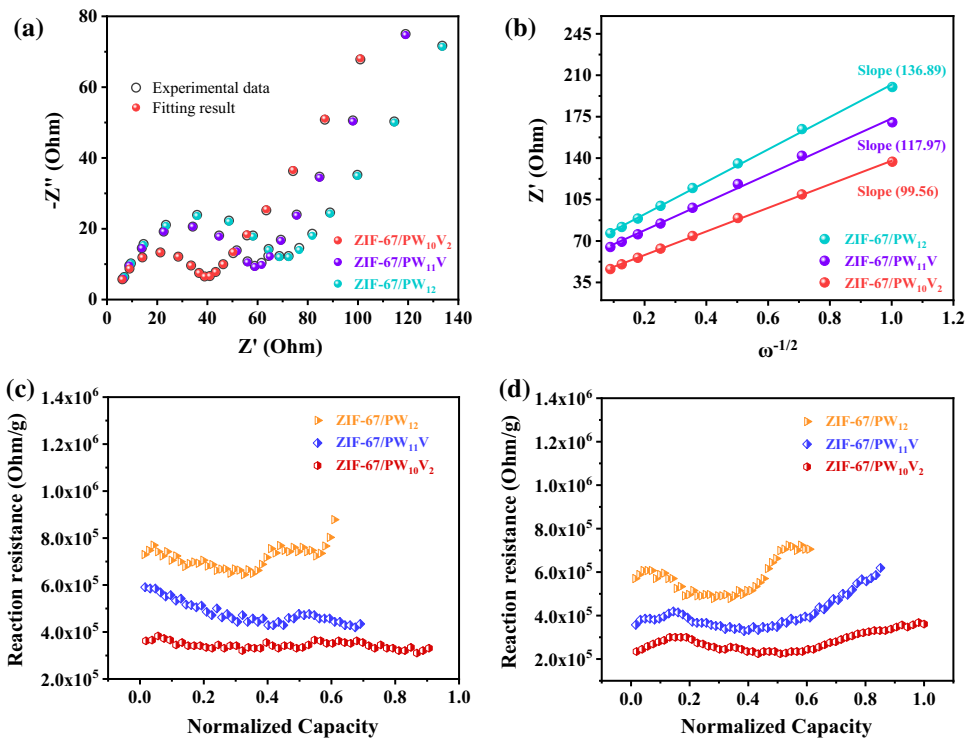

Figure 5 **a** Nyquist plots of ZIF-67/PW_{12}-, ZIF-67/$PW_{11}V$- and ZIF-67/$PW_{10}V_2$-modified separators; **b** the corresponding plots of the real part of impedance (Z') as a function of the inverse square root of the angular frequency ($\omega^{-1/2}$) in the Warburg region; reaction resistance comparison of three ZIF-67/POM-modified separators during the **c** charge process and **d** discharge process.

is the slope of the plot between Z′ with $\omega^{-1/2}$ ($\omega = 2\pi f$), also proves excellent lithium ion transfer efficiency due to $PW_{10}V_2$ catalytic action (Fig. 5b). Besides, we utilize GITT with both transient and steady-state tests to detect reaction resistance evolution of cells with three MOF/POM-modified

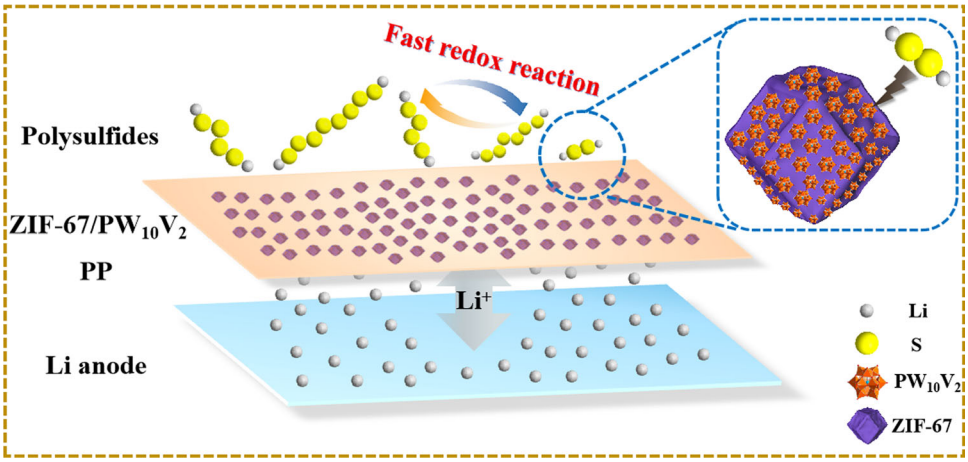

Figure 6 The working mechanism of ZIF-67/$PW_{10}V_2$-modified separator in Li–S cell.

separators (Fig. S21), which is performed by applying current pulses under 0.1 C for 20 min followed by a 120-min relaxation process. Charge–discharge reaction resistances could be analyzed by dividing overpotential with pulse current [37]. As expected, ZIF-67/$PW_{10}V_2$-modified separator displays the lowest reaction resistances in charge/discharge processes (Fig. 5c and d), demonstrating the cell with ZIF-67/$PW_{10}V_2$ presents the excellent electrical conductivity. As a consequence, ZIF-67/$PW_{10}V_2$ as both catalyst layer and barrier layer can prompt the sluggish reaction kinetics of Li–S conversion and prevent polysulfides from shuttling to the lithium anode.

Based on the above discussion, ZIF-67/$PW_{10}V_2$ composite as the modified material of separator in Li–S batteries presents obvious advantages, which are mainly due to the following points (as illustrated in Fig. 6): (1) $PW_{10}V_2$ is tightly and uniformly attached to the surface of ZIF-67 by electrostatic attraction, ensuring the structural stability and synergetic effect of composite; (2) ZIF-67 with suitable size window of micropores acts as a reliable physical barrier to obstruct polysulfides migration, while lithium ions can flow freely across the ZIF-67/$PW_{10}V_2$-modified separator; (3) $PW_{10}V_2$ presents firm chemical affinity and efficient catalytic activity toward polysulfides, which is beneficial to prevent the soluble polysulfides from reaching lithium anode and kinetically accelerate redox reaction of sulfur species during cycling.

Conclusion

This work proposes an available strategy to construct MOF/POM-modified separator, aiming to enhance cycling stability as well as reversible capacity of Li–S cell. ZIF-67 with suitable size window of micropores could function as a reliable physical barrier to restrain polysulfides shuttling, but allow flexible migration of lithium ion. Significantly, $PW_{10}V_2$ combined the merits of excellent catalytic activity and firm adsorption ability plays an essential role in refraining loss of active sulfur material and facilitating redox kinetics of sulfur species. Consequently, the assembled cell with ZIF-67/$PW_{10}V_2$-modified separator achieves an increased specific capacity and outstanding rate performance. This study affords a feasible idea to manufacture functional separator based on the MOF/POM composites for Li–S batteries with remarkable performance. Meanwhile, this research may be spread to other energy systems as well as furnish creative insights into design of electrode materials.

Acknowledgements

We gratefully acknowledge the financial support from the Natural Science Foundation of Shandong Province (ZR2021QB005).

Funding

This study was funded by Natural Science Foundation of Shandong Province, ZR2021QB005, Linlin Fan.

Declarations

Conflict of interest All the authors declare that they have no known competing financial interests or personal relationships that could have appeared to influence the work reported in this paper.

Supplementary Information: The online version contains supplementary material available at https://doi.org/10.1007/s10853-022-07881-7.

References

[1] Mao L, Mao J (2022) Active site construction to boost electrochemical property for Li-S batteries: a review. J Mater Sci 57:7131–7154. https://doi.org/10.1007/s10853-022-07082-2

[2] Zhou G, Li L, Wang D-W, Shan X-Y, Pei S, Li F, Cheng H-M (2015) A flexible sulfur-graphene-polypropylene separator integrated electrode for advanced Li-S batteries. Adv Mater 27:641–647. https://doi.org/10.1002/adma.201404210

[3] Diana MI, Selvasekarapandian S, Selvin PC, Krishna MV (2022) A physicochemical elucidation of sodium perchlorate incorporated alginate biopolymer: toward all-solid-state sodium-ion battery. J Mater Sci 57:8211–8224. https://doi.org/10.1007/s10853-022-07185-w

[4] Wang Q, Deng Y, Ma J, Jin X, Li M, Wu M, Wang Q, Ge B, Zhang L, Liu R (2022) Enhanced sulfur redox kinetics by hollow structured $NiCo_2O_4$ entangled with acidified MWCNTs for lithium sulfur batteries. J Mater Sci 57:4704–4715. https://doi.org/10.1007/s10853-022-06925-2

[5] Hong X, Wang R, Liu Y, Fu J, Liang J, Dou S (2020) Recent advances in chemical adsorption and catalytic conversion materials for Li-S batteries. J Energy Chem 42:144–168. https://doi.org/10.1016/j.jechem.2019.07.001

[6] Zeng M, Wang M, Zheng L, Gao W, Liu R, Pan J, Zhang H, Yang Z, Li X (2022) In situ enhance lithium polysulfides redox kinetics by carbon cloth/MoO_3 self-standing electrode for lithium-sulfur battery. J Mater Sci. https://doi.org/10.1007/s10853-022-07127-6

[7] Ji L, Jia Y, Wang X, Duan L, Li W, Liu J, Zhang Y (2021) Strong adsorption, catalysis and lithiophilic modulation of carbon nitride for lithium/sulfur battery. Nanotechnology 32:192002. https://doi.org/10.1088/1361-6528/abe002

[8] Xiao S, Huang L, Lv W, He Y-B (2022) A highly efficient ion and electron conductive interlayer to achieve low self-discharge of lithium-sulfur batteries. ACS Appl Mater Inter 14:1783–1790. https://doi.org/10.1021/acsami.1c21398

[9] Li Z, Jiao S, Yu D, Zhang Q, Liu K, Han J, Guo Z, Liu J, Wang L (2021) Cationic-polymer-functionalized separator as a high-efficiency polysulfide shuttle barrier for long-life Li-S battery. ACS Appl Energy Mater 4:2914–2921. https://doi.org/10.1021/acsaem.1c00281

[10] Bai S, Liu X, Zhu K, Wu S, Zhou H (2016) Metal-organic framework-based separator for lithium-sulfur batteries. Nat Energy 1:1–6. https://doi.org/10.1038/nenergy.2016.94

[11] Kim SH, Yeon JS, Kim R, Choi KM, Park HS (2018) A functional separator coated with sulfonated metal-organic framework/Nafion hybrids for Li-S batteries. J Mater Chem A 6:24971–24978. https://doi.org/10.1039/c8ta08843h

[12] Yang P, Zhao W, Shkurenko A, Belmabkhout Y, Eddaoudi M, Dong X, Alshareef HN, Khashab NM (2019) Polyoxometalate-cyclodextrin metal-organic frameworks: from tunable structure to customized storage functionality. J Am Chem Soc 141:1847–1851. https://doi.org/10.1021/jacs.8b11998

[13] Pukazhselvan D, Loureiro FJ, Shaula A, Mikhalev S, Bdikin I, Fagg DP (2022) Anatase titania as magnesium host in Mg ion rechargeable battery with magnesium perchlorate/ethylmagnesium bromide electrolytes. J Mater Sci 57:8442–8454. https://doi.org/10.1007/s10853-021-06793-2

[14] Zhao Z, Wang S, Liang R, Li Z, Shi Z, Chen G (2014) Graphene-wrapped chromium-MOF(MIL-101)/sulfur composite for performance improvement of high-rate rechargeable Li–S batteries. J Mater Chem A 2:13509–13512. https://doi.org/10.1039/c4ta01241k

[15] Wang J, Gao L, Zhao J, Zheng J, Wang J, Huang J (2021) A facile in-situ synthesis of ZIF-8 nanoparticles anchored on reduced graphene oxide as a sulfur host for Li-S batteries. Mater Res Bull 133:111061. https://doi.org/10.1016/j.materresbull.2020.111061

[16] Wang Z, Wang B, Yang Y, Cui Y, Wang Z, Chen B, Qian G (2015) Mixed-metal-organic framework with effective lewis acidic sites for sulfur confinement in high-performance lithium-sulfur batteries. ACS Appl Mater Inter 7:20999–21004. https://doi.org/10.1021/acsami.5b07024

[17] Han Z, Li X, Li Q, Li H, Xu J, Li N, Zhao G, Wang X, Li H, Li S (2021) Construction of the POMOF@Polypyrrole composite with enhanced ion diffusion and capacitive contribution for high-performance lithium-ion batteries. ACS Appl Mater Inter 13:6265–6275. https://doi.org/10.1021/acsami.0c20721

[18] Jiang Y, Chen F, Gao Y, Wang Y, Wang S, Gao Q, Jiao Z, Zhao B, Chen Z (2017) Inhibiting the shuttle effect of Li-S battery with a graphene oxide coating separator: performance improvement and mechanism study. J Power Sources 342:929–938. https://doi.org/10.1016/j.jpowsour.2017.01.013

[19] Liu W, Luo C, Zhang S, Zhang B, Ma J, Wang X, Liu W, Li Z, Yang QH, Lv W (2021) Cobalt-doping of molybdenum disulfide for enhanced catalytic polysulfide conversion in lithium-sulfur batteries. ACS Nano 15:7491–7499. https://doi.org/10.1021/acsnano.1c00896

[20] Peng N, Xu G, Jiang J, Zhao A, Liang L (2022) In situ synthesis of core-shell Al@MIL-53 anode for high-

performance lithium-ion batteries. J Mater Sci. https://doi.org/10.1007/s10853-022-07253-1

[21] Mehta V, Saini HS, Srivastava S, Kashyap MK, Tankeshwar K (2022) Ultralow diffusion barrier of double transition metal MoWC monolayer as Li-ion battery anode. J Mater Sci. https://doi.org/10.1007/s10853-022-07237-1

[22] Yao W, Zheng W, Xu J, Tian C, Han K, Sun W, Xiao S (2021) ZnS-SnS@NC Heterostructure as robust lithiophilicity and sulfiphilicity mediator toward high-rate and long-life lithium-sulfur batteries. ACS Nano 15:7114–7130. https://doi.org/10.1021/acsnano.1c00270

[23] Zhang Y, Liu J, Li S-L, Su Z-M, Lan Y-Q (2019) Polyoxometalate-based materials for sustainable and clean energy conversion and storage. EnergyChem 1:100021. https://doi.org/10.1016/j.enchem.2019.100021

[24] Horn MR, Singh A, Alomari S, Goberna-Ferrón S, Benages-Vilau R, Chodankar N, Motta N, Ostrikov K, MacLeod J, Sonar P, Gomez-Romero P, Dubal D (2021) Polyoxometalates (POMs): from electroactive clusters to energy materials. Energ Environ Sci 14:1652–1700. https://doi.org/10.1039/d0ee03407j

[25] Ye J-C, Chen J-J, Yuan R-M, Deng D-R, Zheng M-S, Cronin L, Dong Q-F (2018) Strategies to explore and develop reversible redox reactions of Li-S in electrode architectures using silver-polyoxometalate clusters. J Am Chem Soc 140:3134–3138. https://doi.org/10.1021/jacs.8b00411

[26] Li Z, Xiao D, Xu C, Li Z, Bi S, Xu H, Dou H, Zhang X (2022) MnO_2/carbon nanotube free-standing electrode recycled from spent manganese-oxygen battery as high-performance supercapacitor material. J Mater Sci 57:8818–8827. https://doi.org/10.1007/s10853-022-07223-7

[27] Yu Y, Li T, Zhang H, Luo Y, Zhang H, Zhang J, Yan J, Li X (2020) Principle of progressively and strongly immobilizing polysulfides on polyoxovanadate clusters for excellent Li-S batteries application. Nano Energy 71:104596. https://doi.org/10.1016/j.nanoen.2020.104596

[28] Choi W, Im D, Park MS, Ryu Y-G, Hwang SS, Kim YS, Kim H, Doo S-G, Chang H (2016) Keggin-type polyoxometalates as bidirectional redox mediators for rechargeable batteries. Electrochem 84:882–886. https://doi.org/10.5796/electrochemistry.84.882

[29] Song J, Jiang Y-Y, Lu Y-Z, Wang M-L, Cao Y-D, Fan L-L, Liu H, Gao G-G (2022) Effective polysulfide adsorption and catalysis by polyoxometalate contributing to high-performance Li-S batteries. Mater Today Nano 19:100231. https://doi.org/10.1016/j.mtnano.2022.100231

[30] Ni L, Yang G, Liu Y, Wu Z, Ma Z, Shen C, Lv Z, Wang Q, Gong X, Xie J, Diao G, Wei Y (2021) Self-assembled polyoxometalate nanodots as bidirectional cluster catalysts for polysulfide/sulfide redox conversion in lithium-sulfur batteries. ACS Nano 15:12222–12236. https://doi.org/10.1021/acsnano.1c03852

[31] Duan D, Zhao W, Chen K, Wang Y, Liu S, Zhou X, Chen L, Li Y (2021) MOF-71 derived layered Co-CoP/C for advanced Li-S batteries. J Alloy Compd 886:161203. https://doi.org/10.1016/j.jallcom.2021.161203

[32] Li Z, Zhang Q, Hencz L, Liu J, Kaghazchi P, Han J, Wang L, Zhang S (2021) Multifunctional cation-vacancy-rich $ZnCo_2O_4$ polysulfide-blocking layer for ultrahigh-loading Li-S battery. Nano Energy 89:106331. https://doi.org/10.1016/j.nanoen.2021.106331

[33] Wang J-Y, Qiu W-B, Li G-R, Liu J-B, Luo D, Zhang Y-G, Zhao Y, Zhou G-F, Shui L-L, Wang X, Chen Z-W (2022) Coordinatively deficient single-atom Fe-N-C electrocatalyst with optimized electronic structure for high-performance lithium-sulfur batteries. Energy Storage Mater 46:269–277. https://doi.org/10.1016/j.ensm.2021.12.040

[34] Zhou W, Zhao D, Wu Q, Fan B, Dan J, Han A, Ma L, Zhang X, Li L (2021) Amorphous CoP nanoparticle composites with nitrogen-doped hollow carbon nanospheres for synergetic anchoring and catalytic conversion of polysulfides in Li-S batteries. J Colloid Interf Sci 603:1–10. https://doi.org/10.1016/j.jcis.2021.06.059

[35] Cheng P, Cao D, Fang X, Zhao Y, Cao P, Liu D, He D (2022) Enhanced immobilization and accelerated conversion of polysulfides by functionalized separator for advanced lithium sulfur batteries. J Power Sources 539:231490. https://doi.org/10.1016/j.jpowsour.2022.231490

[36] Xian C, Jing P, Pu X, Wang G, Wang Q, Wu H, Zhang Y (2020) A trifunctional separator based on a blockage-adsorption-catalysis synergistic effect for Li-S batteries. ACS Appl Mater Inter 12:47599–47611. https://doi.org/10.1021/acsami.0c14645

[37] Li M, Wan Y, Huang J-K, Assen AH, Hsiung C-E, Jiang H, Han Y, Eddaoudi M, Lai Z, Ming J, Li L-J (2017) Metal-organic framework-based separators for enhancing Li-S battery stability: mechanism of mitigating polysulfide diffusion. ACS Energy Lett 2:2362–2367. https://doi.org/10.1021/acsenergylett.7b00692